

MULTICHANNEL SEISMIC EVIDENCE FOR VARIATIONS IN CRUSTAL THICKNESS
ACROSS THE MOLOKAI FRACTURE ZONE IN THE MID-PACIFIC

Uri S. ten Brink¹

Lamont-Doherty Geological Observatory and Department of Geological Sciences
Columbia University, Palisades, New York

Thomas M. Brocher

U.S. Geological Survey, Menlo Park, California

Abstract. Coincident multichannel seismic reflection and refraction data from a N-S transect near Oahu, Hawaii, provide evidence for thickening of the Pacific crust by $1-2 \pm 1$ km south of the large-offset (16 m.y.) Molokai Fracture Zone (FZ). Tau-p stacks, tau-sum inversions, and forward modeling of the refraction data indicate that the crustal thickening occurs primarily within the lower portion of seismic layer 2. Assuming isostatic balance, the differences in crustal thickness predict that seafloor having the same age will have different elevations across the FZ. Observations of seafloor depths across the FZ east of the Hawaiian Islands are consistent with this prediction implying that the processes which have generated the crustal differences have been stable for over 50 m.y. Previous correlations between the chemical composition of ridge crest basalts, crustal thickness, and ridge crest elevation have been attributed to variations in the thermal regime of the upper mantle under mid-ocean spreading centers. In accord with this hypothesis, we propose that the observed differences in crustal structure across the Molokai FZ may have been produced by small (25°C) differences in the thermal regime of the upper mantle beneath the ancestral East Pacific Rise. Discontinuous intracrustal reflections located about 1.6 s below the sediment/basement interface are observed in migrated reflection data south of Oahu. These reflections are similar in character to the lower crustal "Horizon R" event observed in the western North Atlantic. Shallower intracrustal reflections, possibly from within seismic layer 2, are also observed. The observation of these intracrustal reflections in both the Atlantic and Pacific oceans suggests that they are a fundamental signature of the crustal accretion process at a variety of spreading rates and that they are mappable using modern seismic reflection/refraction methods.

Introduction

The seismic structure of the oceanic crust has been revealed over the past two decades by using

¹Now at Department of Geophysics, Stanford University, Stanford, California.

Copyright 1988 by the American Geophysical Union.

Paper number 7B5020.
0148-0227/88/007B-5020\$05.00

seismic refraction techniques. These refraction studies indicate a continuous change of seismic velocities with depth into the crust which may be subdivided into (1) a high-velocity gradient (1 s^{-1}) layer in the upper crust (seismic layer 2) and (2) a reduced velocity gradient (0.1 s^{-1}) layer in the lower crust (seismic layer 3) [e.g., Spudich and Orcutt, 1980; Kempner and Gettrust, 1982; Purdy and Ewing, 1986]. Interpretations of these velocities based on ophiolites, thought to represent obducted or accreted fragments of oceanic crust, and oceanic drilling results suggests that the upper crust (layer 2) consists of extrusive basalt and brecciated dikes [Anderson et al., 1982], and that the lower crust (layer 3) is a massive gabbro plutonic section. Furthermore, sheeted dykes are replaced by isotropic gabbros in the transition between the basalts and gabbros [Salisbury and Christensen, 1978; Bratt and Purdy, 1984]. The Moho is typically modeled on seismic refraction sections as either a first-order discontinuity or a linear velocity gradient (transition zone) up to 2 km thick [Spudich and Orcutt, 1980]. This transition is often interpreted as a petrologic gradient having an increasing percentage of ultramafic rocks with depth [Cann, 1974; Christensen, 1978; Fox and Stroup, 1981; Spudich and Orcutt, 1980; Kempner and Gettrust, 1982].

Models for the origin and evolution of the oceanic lithosphere depend on the determination of structural variations of the oceanic crust in many tectonic settings. As noted by other investigators [e.g., NAT Study Group, 1985], combined seismic reflection/refraction experiments offer a unique ability to resolve these variations due to their ability to provide both velocity information as well as high-resolution images of the crust.

We report results from a combined wide-aperture two-ship multichannel seismic reflection/refraction experiment carried out during August-September 1982 near Oahu, Hawaii, by the Lamont-Doherty Geological Observatory and the Hawaii Institute of Geophysics (Figure 1). Multichannel seismic refraction profiles and coincident and crossing multichannel seismic reflection profiles acquired during this experiment allow the detailed examination of spatial variations in layers 2 and 3 and the crust-mantle transition in "normal" Pacific crust having ages between 60 and 80 m.y. [Atwater and Menard, 1970]. The lower crust has apparently been altered by the hotspot-related volcanism as far as 100 km from the center of Oahu [ten Brink and Brocher, 1987]; hence we describe that portion of the data set where the crust appears

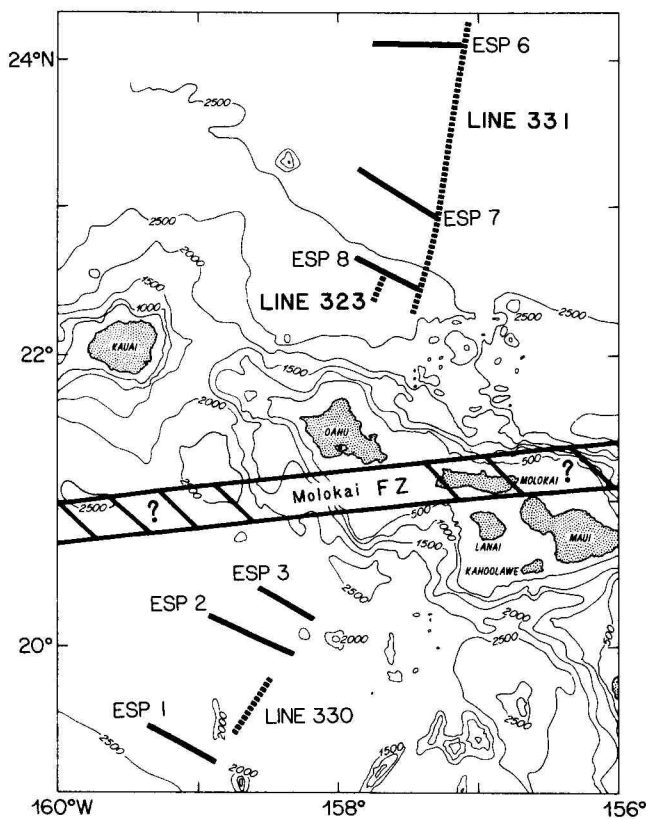


Fig. 1. Location map of Expanding Spread Profiles (ESPs) and CDP reflection lines 323, 330, and 331 cited in the text. Bathymetry is contoured at 500-fathom intervals (1 fathom = 1.8288 m) and is based on work by Chase et al. [1970]. The location of the Molokai FZ shown in this figure is approximate.

to be normal in both thickness and structure. We examine the variability in the seismic structure of the oceanic crust and relate this variability to the Molokai Fracture Zone.

Data Acquisition

Six Expanding Spread Profiles (ESPs), with an average latitudinal spacing of 73 km, were recorded using airgun array and explosive sources located as far as 60–95 km from the multichannel receiver (Table 1). The ESPs were oriented parallel to the trend of the chain to minimize lateral variations introduced by lithospheric flexure (Figure 1). Their orientation is thus oblique to the N–S trending isochrons of the seafloor identified east of the Hawaiian Islands. The structure under these ESPs was further controlled by vertical and wide-angle reflection profiles collected coincident with each ESP and along lines acquired perpendicular to the orientation of the ESPs. Further information concerning data acquisition and preliminary data processing is provided in Watts et al. [1985], Brocher and ten Brink [1987], and ten Brink and Brocher [1987]. Timing and range

corrections and uncertainties are discussed by ten Brink [1986].

Processing and Analysis of Expanding Spread Profiles

A variety of methods were used to analyze the ESP data. Each ESP was collected twice, once using explosive sources to ranges no smaller than 25 km and once with an airgun array to smaller ranges (Table 1). The two different types of ESP data were reduced independently from one another. The ESPs acquired using airgun and explosive sources were merged to provide refraction records containing arrivals from ranges of 0 to 60–95 km (e.g., Figure 2). Where the ESPs were spliced together, arrivals on adjacent traces of the merged ESPs generally agree to within 20 ms.

Interpretation of the ESPs followed the procedure described by ten Brink and Brocher [1987] which, because of the generally minor and smooth topography along the profiles, assumed a laterally homogeneous structure. The ESPs were first inverted for velocity-depth structure using the recursive tau-sum method [Diebold and Stoffa, 1981]. Low signal-to-noise ratios on the tau-p stacks, however, often made the identification of the principal arrivals on the tau-p curve difficult. To improve our ability to identify these arrivals, a semblance threshold (of less than 0.17 in the near offsets and less than 0.1 in the far offsets) was applied to the tau-p stacks, as described by Diebold and Stoffa [1981].

Given the difficulties introduced by noise on the tau-p stacks, these velocity-depth solutions were used as initial inputs for forward modeling of travel times assuming laterally homogeneous media. While all parts of the travel time curve were fit as accurately as possible, the ranges to the critical points of the PmP branches and to the crossover distances between the crustal and Pn branches were particularly carefully matched (Figure 2). Additional constraints on a few of the velocity-depth solutions were provided by the vertical two-way travel time (TWTT) of Moho reflections in Common-Depth Point (CDP) reflection lines coincident with and orthogonal to the ESPs (Table 2).

Synthetic seismograms calculated by the WKBJ method [Chapman, 1978] were used to refine the

TABLE 1. ESP Acquisition Parameters

| ESP | Range of Airgun, Explosive Sources for ESPs, km | Explosive Size, kg | Azimuth, deg |
|-----|---|--------------------|--------------|
| 1 | 0–62.3, 16.8–63.2 | 27 | 121 |
| 2 | 0–72.4, 30–82 | 27 | 114 |
| 3 | 0–89.3, 28.9–94.7 | 27 | 120 |
| 6 | 0–60.0, 34–73.7 | 14 | 092 |
| 7 | 0–61.3, 28.2–68.3 | 14 | 123 |
| 8 | 0–82.5, 32.1–64 | 14 | 114 |

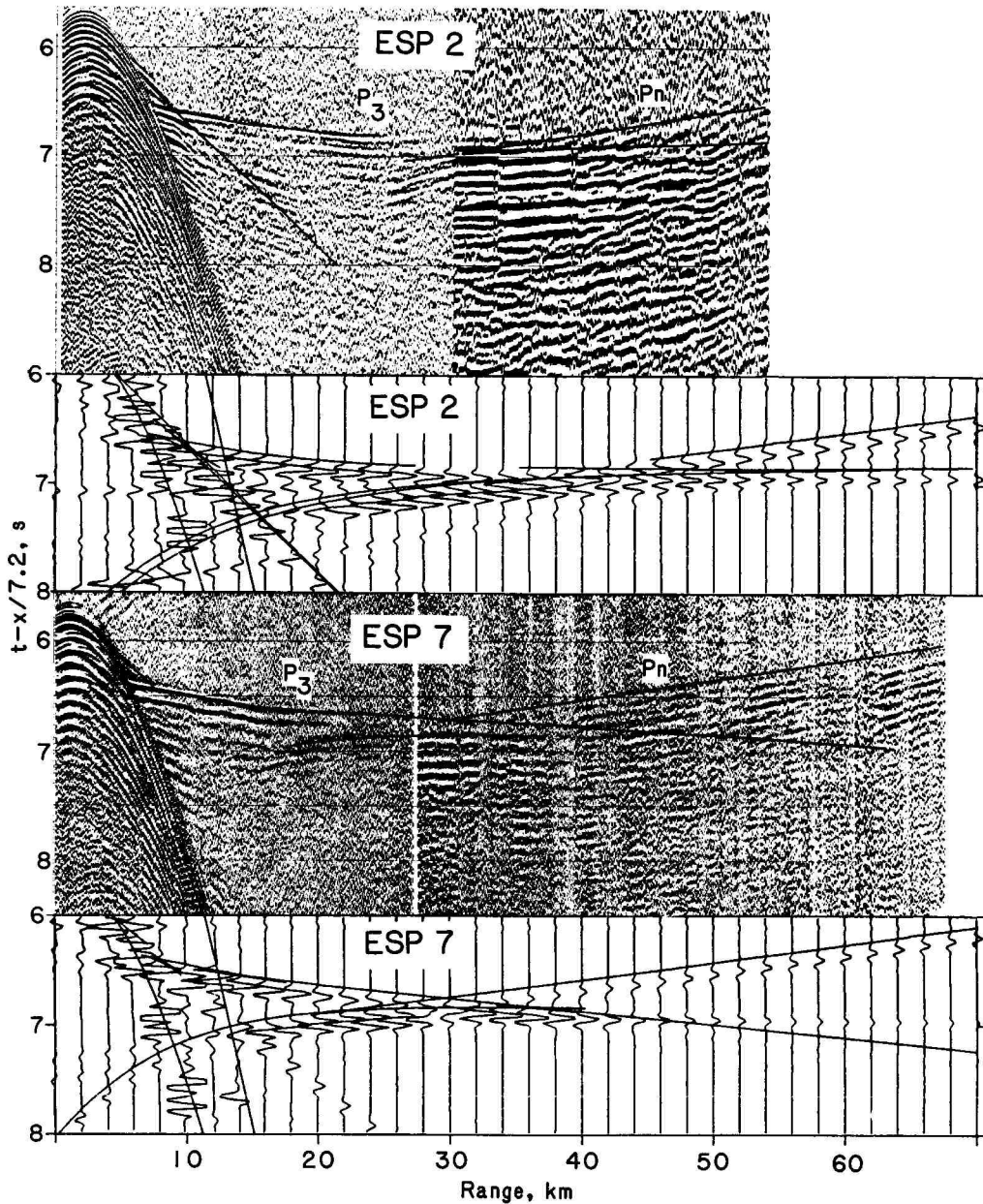


Fig. 2. Examples of ESPs shot over the two different types of crust found along the transect. The travel times of both ESPs are reduced by 7.2 km/s; both ESPs have been plotted using identical parameters. ESP 7 is located north of Oahu; ESP 2 is located south of Oahu (Figure 1). Thin solid lines show calculated travel times for the velocity-depth models listed in Table 2. The change in signal character observed on both records at ranges of approximately 30 km originates from the change from an airgun to an explosive source at this range. Also shown are predicted travel times and synthetic seismograms calculated using WKBJ theory [Chapman, 1978] for the models of the ESPs listed in Table 2. The synthetics, also plotted without range scaling, successfully match the amplitude-range behavior of the crustal P_3 branch, the location and width of the P_mP arrival, and the relative amplitudes of the P_n and P_mP arrivals for ranges greater than 40 km. The signal-to-noise (S/N) ratio of these ESP data is slightly higher than the average S/N of the ESP data examined in this study.

solutions. The synthetic seismograms successfully match the amplitude-range behavior of the lower crustal P_3 branch, the width and location of the P_mP branch, and the relative amplitudes of P_n and P_mP arrivals for ranges greater than 40 km.

Interpretation

The ESPs were divided into two groups consisting of profiles collected north and south of Oahu, respectively, to highlight the charac-

TABLE 2. ESP Solutions From Forward Modeling

| Layer | TWTT, s | | Vp, km/s | | Depth, km |
|--------------|----------|------------|----------|------|-----------|
| | Observed | Calculated | Top | Base | |
| <u>ESP 1</u> | | | | | |
| 1 | | | 1.5 | 1.5 | |
| 2 | 5.90 | 5.99 | 1.5 | 1.6 | 4.50 |
| 3 | | 6.24 | 4.2 | 5.7 | 4.70 |
| 4 | | 6.48 | 5.7 | 6.0 | 5.25 |
| 5 | | 6.61 | 6.0 | 6.9 | 5.65 |
| 6 | | 7.20 | 6.9 | 7.2 | 7.55 |
| 7 | 8.12 | 8.05 | 7.2 | 8.3 | 10.55 |
| <u>ESP 2</u> | | | | | |
| 1 | | | 1.5 | 1.5 | |
| 2 | 5.85 | 5.87 | 1.7 | 1.7 | 4.40 |
| 3 | | 5.91 | 3.9 | 3.9 | 4.43 |
| 4 | | 5.98 | 3.9 | 3.9 | 4.57 |
| 5 | 6.25 | 6.32 | 4.2 | 4.9 | 5.23 |
| 6 | | 6.76 | 4.9 | 6.1 | 6.23 |
| 7 | | 6.83 | 6.1 | 6.2 | 6.41 |
| 8 | | 6.89 | 6.2 | 6.6 | 6.60 |
| 9 | | 7.17 | 6.6 | 6.7 | 7.49 |
| 10 | | 7.31 | 6.7 | 7.1 | 7.95 |
| 11 | | 7.68 | 7.2 | 7.3 | 9.23 |
| 12 | | 8.48 | 7.4 | 8.1 | 12.15 |
| <u>ESP 3</u> | | | | | |
| 1 | | | 1.5 | 1.5 | |
| 2 | 5.93 | 5.93 | 3.4 | 3.4 | 4.45 |
| 3 | 6.43 | 5.95 | 4.0 | 4.0 | 4.48 |
| 4 | | 6.42 | 4.3 | 4.7 | 5.43 |
| 5 | | 6.50 | 4.7 | 5.1 | 5.61 |
| 6 | | 6.71 | 5.1 | 5.6 | 6.13 |
| 7 | | 6.82 | 5.6 | 5.7 | 6.42 |
| 8 | | 6.95 | 5.9 | 6.2 | 6.79 |
| 9 | | 7.30 | 6.3 | 6.8 | 7.84 |
| 10 | | 7.55 | 6.8 | 7.1 | 8.66 |
| 11 | | 7.80 | 7.1 | 7.3 | 9.53 |
| 12 | | 8.74 | 7.3 | 7.9 | 12.86 |
| 13 | | 9.25 | 7.9 | 8.3 | 13.10 |
| <u>ESP 6</u> | | | | | |
| 1 | | | 1.5 | 1.5 | |
| 2 | 5.85 | 5.85 | 1.5 | 1.6 | 4.40 |
| 3 | 6.00 | 6.12 | 4.2 | 5.7 | 4.60 |
| 4 | | 6.23 | 5.7 | 6.2 | 5.10 |
| 5 | | 6.48 | 6.2 | 6.3 | 5.57 |
| 6 | | 6.62 | 6.3 | 6.4 | 5.97 |
| 7 | | 6.73 | 6.4 | 6.7 | 6.37 |
| 8 | | 7.41 | 6.7 | 6.9 | 8.59 |
| 9 | | 7.88 | 6.9 | 8.3 | 10.20 |
| <u>ESP 7</u> | | | | | |
| 1 | | | 1.5 | 1.5 | |
| 2 | 5.96 | 5.97 | 3.7 | 4.3 | 4.45 |
| 3 | | 6.06 | 4.3 | 4.4 | 4.68 |
| 4 | | 6.12 | 4.2 | 4.2 | 4.82 |
| 5 | 6.25 | 6.32 | 4.5 | 5.1 | 5.24 |
| 6 | | 6.62 | 5.1 | 6.1 | 5.80 |
| 7 | | 6.64 | 6.1 | 6.4 | 6.01 |
| 8 | | 6.97 | 6.5 | 6.6 | 6.90 |
| 9 | | 7.18 | 6.6 | 6.6 | 7.53 |
| 10 | | 7.29 | 6.6 | 7.2 | 8.11 |
| 11 | | 8.02 | 7.2 | 7.8 | 10.80 |

TABLE 2. (continued)

| Layer | TWTT, s | | Vp, km/s | | Depth, km |
|--------------|----------|------------|----------|------|-----------|
| | Observed | Calculated | Top | Base | |
| <u>ESP 8</u> | | | | | |
| 1 | | | 1.5 | 1.5 | |
| 2 | 6.35 | 6.35 | 1.7 | 1.7 | 4.79 |
| 3 | | 6.40 | 4.2 | 4.4 | 4.83 |
| 4 | | 6.63 | 4.3 | 4.3 | 5.32 |
| 5 | 6.90 | 6.77 | 4.3 | 4.4 | 5.63 |
| 6 | | 7.11 | 4.7 | 5.7 | 6.35 |
| 7 | | 7.17 | 5.9 | 6.1 | 6.52 |
| 8 | | 7.36 | 6.4 | 6.5 | 7.09 |
| 9 | | 7.53 | 6.6 | 6.9 | 7.64 |
| 10 | | 7.74 | 6.9 | 7.1 | 8.33 |
| 11 | 8.65 | 8.78 | 7.2 | 7.9 | 11.93 |

teristics of each group and the differences between them. These differences define variations in the crustal structure between two segments of the mid-Pacific plate separated by the Molokai Fracture Zone. We next discuss characteristic differences between the two groups of ESPs, first as observed in the offset-travel time ($x-t$) domain, and then as observed in the intercept time-ray parameter ($\tau-p$) domain. The following section discusses the igneous crust below the upper 1 km, since Brocher and ten Brink [1987] described and interpreted the near-field portion of the refraction records corresponding to arrivals from the sediments and the upper 1 km of the igneous crust. For the purpose of discussion in this paper we define layer 3 as the low-velocity gradient (less than 0.1 s⁻¹) region at the bottom of the crust [Spudich and Orcutt, 1980; Fox and Stroup, 1981].

The first group of ESPs (1, 2, and 3) are located south of Oahu (Figure 1). Compressional wave arrivals on these ESPs are characterized by a single strongly curved crustal refraction (branch P₃) observed to distances of as large as 26 km. At ranges of 20–26 km the P₃ branch has phase velocities of 7.2 km/s. Branch P₃ is typical of an arrival from a series of velocity gradients whose magnitudes progressively decrease with depth.

The second group of ESPs (6, 7, and 8) are located north of Oahu (Figure 1). P₃ arrivals on ESPs acquired north of Oahu differ from those collected south of Oahu in having lower phase velocities which are observed to smaller ranges (Figure 2). These profiles are in general of poorer quality than the profiles acquired south of Oahu because rougher seas and problems with the multichannel receiver were encountered north of Oahu and because smaller explosive charge sizes were used north of Oahu (Table 1).

The $\tau-p$ stacks of the ESPs allow an objective comparison of the crustal structure between groups 1 and 2. The structure within the igneous crust is more easily compared after subtracting the contributions of the water and sedimentary layers, as defined by Brocher and ten Brink [1987], from the intercept times of each $\tau-p$ stack:

$$\tau(p)_{\text{corrected}} = \tau(p) - 2Z (V_2 - p_2) / 2$$

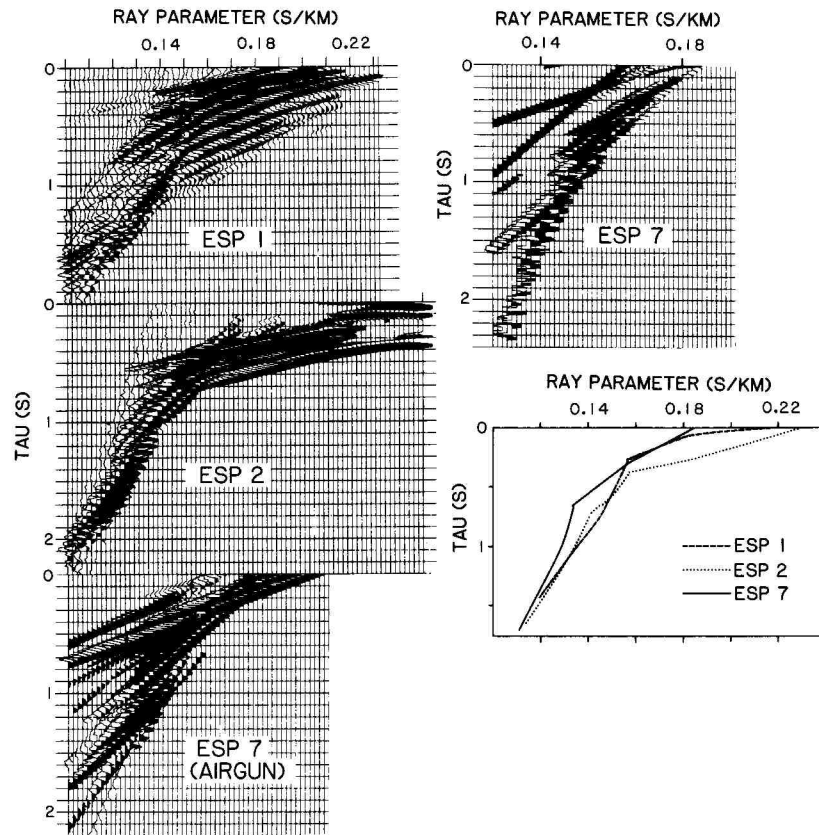


Fig. 3. Comparison of the tau-p stacks and tau-p curves for several ESPs discussed in the text. Note that two tau-p stacks are shown for ESP 7, one for the profile obtained using only airgun sources, and the other for the merged profile obtained using both airgun and explosive sources. Each tau-p stack has been corrected for the water depth and sediment thickness at the ESP midpoint as described in the text. Tau=0 s corresponds to the top of the igneous crust. The line diagram in the lower right-hand corner compares the tau-p curves corresponding to the principal branches of the arrivals chosen from the tau-p stacks.

where V and Z are the velocity and thickness of each layer to be removed and p is the ray parameter. In the case of a layer having a linear velocity gradient, the layer was subdivided into a number of 10-m-thick layers, each having a constant velocity. For the velocity models listed in Table 2 this approximation differs by less than 2 ms from the exact analytical calculation for linear velocity gradients.

The tau-p stacks, corrected for the water and sediment layers listed in Table 2, show systematic variations between groups 1 and 2 (Figure 3). The curves of minimum tau on the tau-p stacks are interpreted as corresponding to the principal branches, while subsequent curves in the tau-p stacks which parallel the principal arrivals are interpreted as originating from the reverberant source waveform and/or multiple arrivals. The principal postcritical arrivals for each ESP, shown in the lower right-hand corner of Figure 3, indicate systematic variations in crustal thickness.

Tau-p curves having a smaller intercept time at the smaller ray parameters indicate a thinner crust. Figure 3 demonstrates that the total crustal thickness of ESP 7 is significantly

smaller than that of ESP 2 and slightly smaller than that of ESP 1. Differences of up to 0.22 s between the intercept times of the principal tau-p branches of ESPs 2 and 7 are generated in the upper to middle part of the crust (p larger than 0.17 s/km, corresponding to velocities smaller than 6 km/s) and are maintained throughout the crust. Differences between the tau-p curves for ESP 1 and 7 originate at $p = 0.156$ s/km (corresponding to velocity of 6.4 km/s) and suggest a slightly thicker middle crust for ESP 1 than for ESP 7. These differences indicate that layer 2 is thickest south of Oahu.

ESP Solutions

Velocity-depth solutions for the ESPs, shown in Figure 4 and listed in Table 2, also show systematic variations in crustal thickness. We adopted the solutions of Brocher and ten Brink [1987] for the sediments and upper igneous crust. The agreement between the tau-sum and forward solutions, the observed and calculated travel times in Figure 5, and the observed and calculated amplitude-range distributions in Figure 2 support the conclusion that the solutions represent an accurate model for the crustal

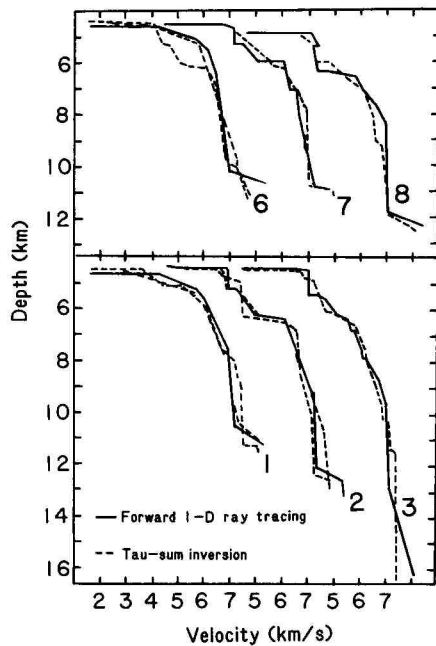


Fig. 4. Summary of velocity-depth solutions for the ESPs discussed in the text. Numbers refer to ESP numbers. Solutions obtained using tau-sum inversion (dashed lines) of the tau-p stacks are compared to solutions obtained from iterative travel time modeling (solid lines). Multiple tau-sum solutions for some ESPs represent differing inversion results obtained using alternative principal branch curves chosen from the tau-p stack of the ESP.

structure near Oahu. Despite the lack of formal extremal bounds on the velocity-depth solutions, comparison of the variability of the tau-sum and forward models in Figure 4 suggests that the depth to the upper mantle is constrained to within ± 0.5 km and that the uncertainty in the velocity of the lower 2-3 km of the crust is about ± 0.3 km/s.

The P₃ branch in the group 1 profiles is best modeled by a monotonic decrease in velocity gradient. However, amplitude-range variations along P₃ require a few constant gradient layers 0.5-1.0 km thick (e.g., the solution for ESP 2) (Figure 4). Velocities for the group 2 solutions in general fluctuate more rapidly with depth than those of group 1. Velocity discontinuities and/or high-velocity gradients were required to match rapid changes in phase velocity and amplitude observed along P₃ on group 2 profiles.

Forward modeling of both travel times and amplitudes suggests that the layer 3 velocity in the lower plutonic section may be higher for group 1 than group 2 (7.2 versus 6.9 km/s). Both the lower phase velocity at the farthest observed offset of branch P₃ in group 2 relative to group 1 profiles and the smaller critical distance of PmP in group 2 compared to group 1 profiles suggest that layer 3 has different velocities north and south of Oahu. It is difficult, however, to verify this difference through comparison of the tau-p stacks shown in Figure 3.

The thickness of layer 3 varies from 2.5 to 3.5 km in both group 1 and 2 ESPs and is best constrained when observable Moho reflections are present on the ESPs: otherwise the layer 3 thickness was constrained by the TWTT to the Moho reflection observed on crossing CDP lines. On the average, layer 3 may be thicker by a few hundred meters south of the Hawaiian Ridge than north of it, but the data do not confidently resolve this difference in thickness (Figure 6).

Intracrustal Reflections

Intracrustal reflections are identified in four CDP lines obtained along our transect: all four lines are located south of Oahu. Because data quality of the CDP profiles is generally higher to the south of Oahu than to the north, we attribute this observation more to variations in data quality than to true structural variability.

CDP line 330, spanning the flexural arch south of Oahu (Figure 1), shows two sets of possible intracrustal reflections on both migrated and unmigrated stacks of the section (Figure 7). The

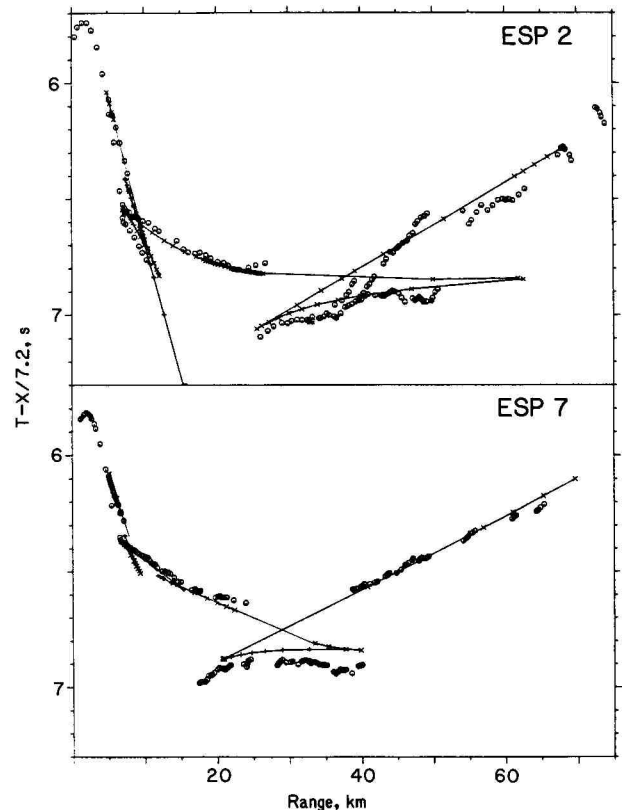


Fig. 5. Comparison of observed and calculated travel times for ESPs 2 and 7. The travel times of both ESPs are reduced by 7.2 km/s. Open circles represent the observed travel times, solid lines connect calculated travel times shown as crosses. For ESP 2 the travel times near the 30-km range were adjusted to account for an observed thinning of the sediment cover at this range in the coincident CDP reflection profile. The travel times for ESP 2 at ranges greater than 47 km were corrected to account for an abyssal hill.

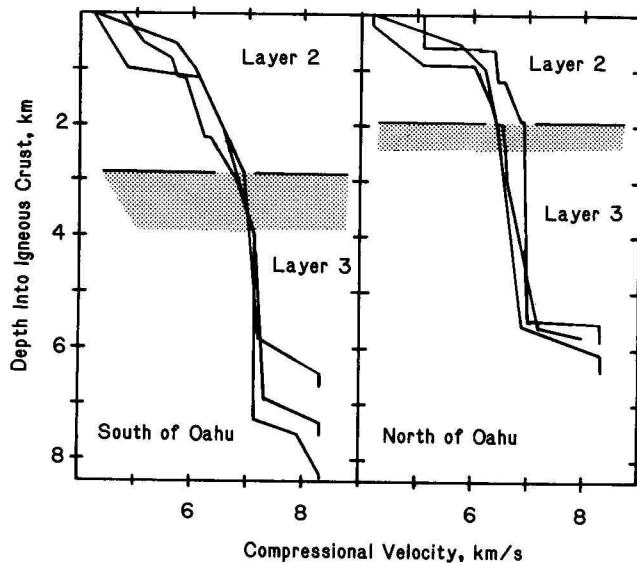


Fig. 6. Comparison of velocity-depth solutions obtained from forward modeling of ESPs acquired north and south of Oahu. Only portions of the solutions corresponding to the igneous crust are shown. The shaded region corresponds to the range of depth to the top of seismic layer 3 (having a reduced velocity gradient) inferred from these solutions.

more prominent of these reflections at 7.5 s TWTT define an undulatory subhorizontal surface in the lower crust about 1.6 s beneath the sediment-basement interface. ESP data confirm that the

Moho transition is at 8.0–8.2 s TWTT, more than 0.5 s below the lower crustal reflection. A second, shallower and discontinuous reflection at 6.3–6.5 s TWTT (Figure 8) is located 0.5–1.0 s below the sediment-basement contact. The velocity models for ESPs 1 and 2 suggest that these reflections are generated within layer 2 (Table 2).

We believe that these events are reflected from the midcrust to lower crust. The intracrustal reflections shown in Figures 7 and 8 stack well at velocities appropriate for midcrustal reflections. Because Tsai [1984] has shown that side scatterers from the seafloor or the rugged sediment-basement interface may also have high stacking velocities, it is necessary to check the frequency content of potential intracrustal reflections. Poststack tests of the frequency content of a portion of line 330, shown in Figure 9, indicate that these intracrustal reflection events do not have high-frequency contents appropriate for predominately waterborne signals. Although they have a higher-frequency content than the events from the Moho transition, these events lack coherent energy above 20 Hz typical of the seafloor or first multiple reflections shown in Figure 9.

Discussion

Our analyses indicate a significant difference in crustal thickness between groups 1 and 2 (Figure 6) with the total crustal section north of Oahu being generally about 1–2 + 1 km thinner than that south of Oahu. Velocity-depth solutions for ESPs located south of Oahu vary in

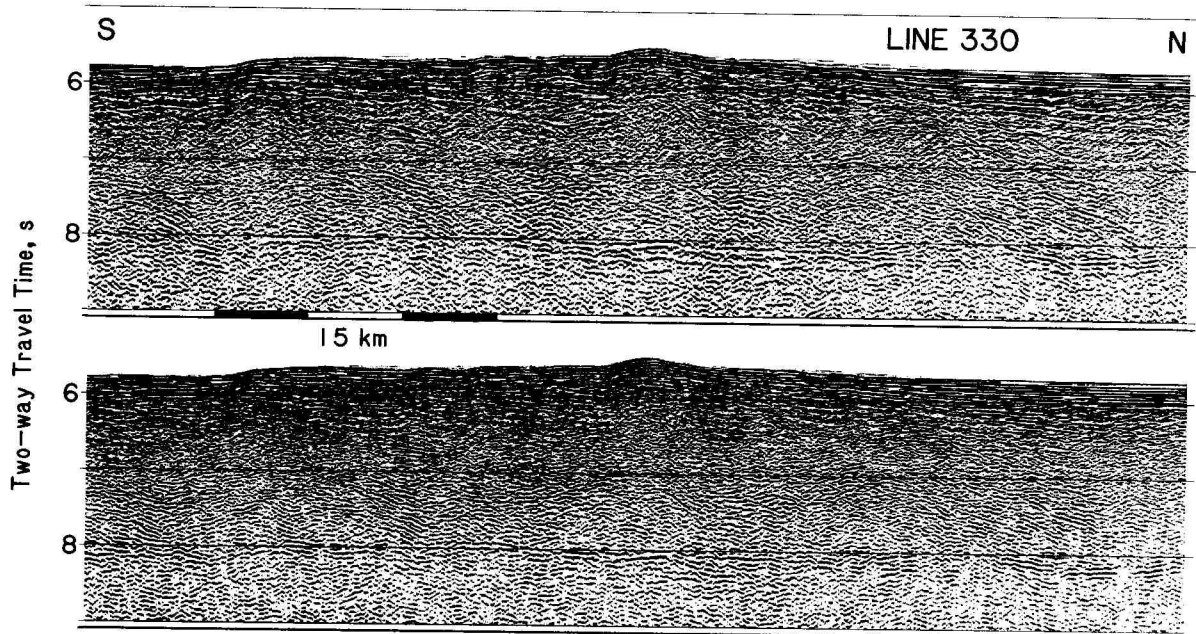


Fig. 7. A segment of CDP line 330 collected south of Oahu showing intracrustal reflections: in the top part of the figure the section is unmigrated, in the bottom part of the figure the section has been migrated using a 450 finite difference algorithm and migration velocities which varied with depth and distance along the section. Intracrustal reflections occur at approximately 7.5 s TWTT. The Moho reflection is typically observed between 8.0 and 8.2 s TWTT along this portion of the section. Both sections were band-pass filtered 5–15 Hz and were corrected for spherical divergence.

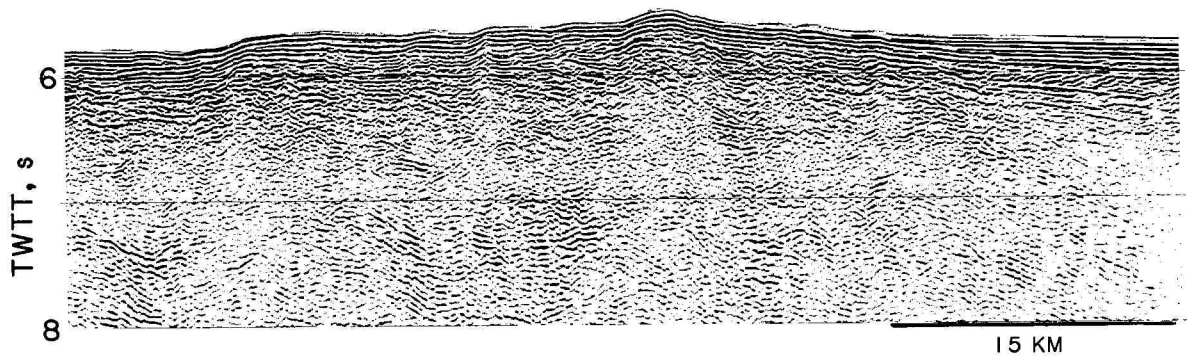


Fig. 8. Expanded plot of the migrated data of line 330 shown in Figure 7, plotted without automatic gain control to preserve relative trace-to-trace amplitude relationships. Note the intracrustal reflections at 6.5 and 7.5 s TWTT.

total crustal thickness between 6.5 and 8.2 km, whereas north of Oahu they are 5.5 to 6.1 km thick (Figure 6). These results are in agreement with those of Furumoto et al. [1968], who reported a similar asymmetry in total crustal thickness north and south of Oahu. Comparison of CDP profiles located north and south of Oahu supports this conclusion (Figure 10).

Inspection of the tau-p stacks (Figure 3) as well as the ESP velocity-depth solutions (Figure 6) suggest that the difference in crustal thick-

ness is, in large part, due to layer 2 being about 1.0 ± 0.5 km thinner to the north of Oahu than to the south. As previously discussed, the forward modeling suggests, but objective measures do not require, that the Layer 3 velocity north of Oahu may be 5 percent slower than to the south of Oahu. We emphasize that the observed differences in crustal structure north and south of Oahu can not be related to differences in the water depth or to the structure of the upper crust, since direct comparison of ESP 7 with ESP

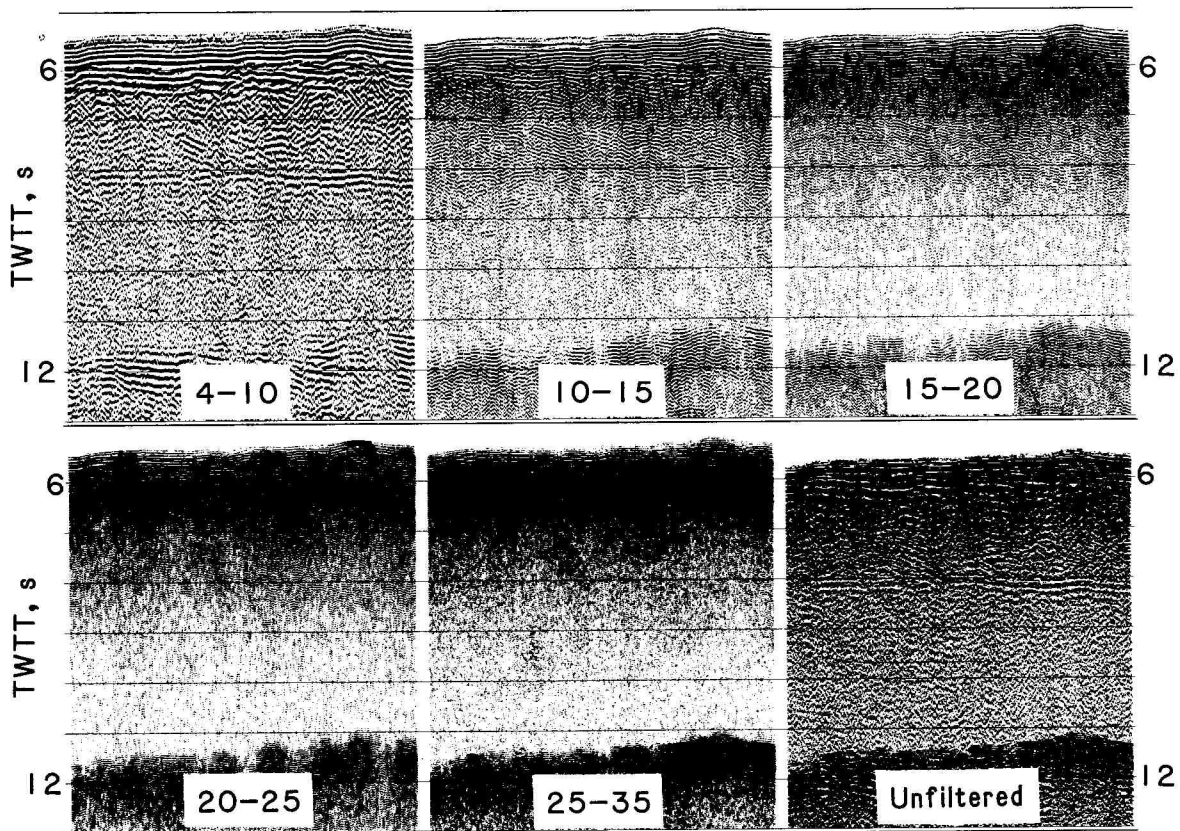


Fig. 9. A test of the frequency content of the intracrustal reflections using the narrow frequency band-pass filters indicated (numbers are in hertz) on a short segment of CDP line 330. A 2-Hz-wide side taper was applied to the band-pass filters in all cases. The unfiltered section is shown for comparison in the lower right corner.

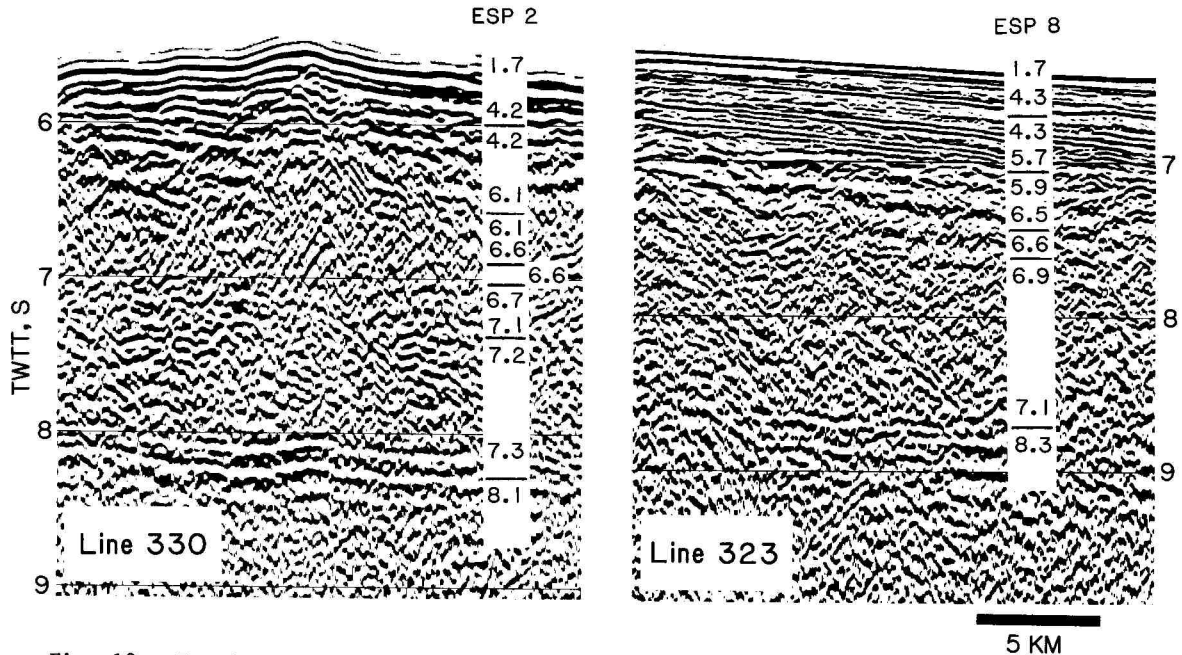


Fig. 10. Portions of CDP reflection lines 323 and 330 comparing the crustal thickness (in TWTT) at vertical incidence. Locations of these sections are shown on Figure 1. Both sections were band-pass filtered between 5 and 15 Hz and were plotted using automatic gain control. Velocities (in kilometers per second) inferred from the closest available ESPs (2 and 8) are superimposed on these sections using calculated travel times provided in Table 2. Because the ESPs and the CDP reflection sections are not coincident, the calculated travel times have been shifted to match the seafloor reflection time.

2, collected in similar water depths and having similar sediment cover and upper crustal structures [Brocher and ten Brink, 1987], shows differences in the middle to lower crustal arrivals (Figure 2).

The seismic variations observed north and south of Oahu could be explained by two crustal segments separated by a fracture zone (Figure 11). The Molokai Fracture Zone (FZ) separates segments of seafloor having different ages north and south of Oahu (Figure 1). Extrapolation of seafloor ages north and south of Oahu from the

last observed magnetic anomaly (anomaly 32) places the ages of these segments at about 64 Ma and 80 Ma north and south of the island, respectively [Atwater and Menard, 1970]. The age contrast is not much altered by the fact that the ESPs were shot at an oblique angle to the isochrons, because considering their length (less than 100 km) and the fast spreading rate of the mid-Pacific, each ESP covers seafloor generated within a period of less than 1 m.y and each group of ESPs (north and south of Oahu) covers a time period of less than 2 m.y.

As its name indicates, the Molokai FZ probably crosses the Hawaiian Islands in the vicinity of Molokai. The FZ is likely to be responsible for the lineated bathymetric pattern trending W-NW found on the carbonate platform east of Molokai [Fornari and Campbell, 1987]. The principal trends of the subaerial and submarine rift zones of the east and west Molokai volcanoes are parallel to the FZ and were interpreted to be partly controlled by it [Malahoff and Woollard, 1968]. The exact location of the Molokai FZ across the Hawaiian chain cannot, however, be determined because the bathymetric and gravity signatures of the Molokai FZ disappear in the flexural moat north of the Hawaiian Islands and cannot be traced with confidence to the southwest of the islands. Moreover, the island chain is located in the Cretaceous magnetic quiet zone. The trace of the Molokai FZ was also not identified on the seismic reflection data acquired during our experiment.

Crustal thicknesses similar to the ones found north of Oahu are reported from two other seismic

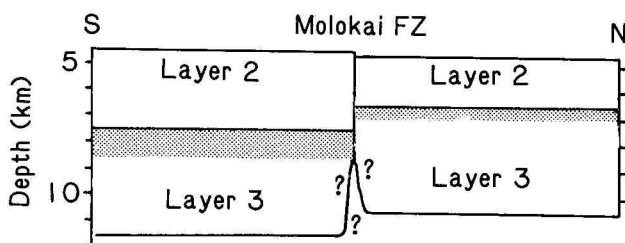


Fig. 11. Schematic model of the crustal structure across the Molokai Fracture Zone (FZ). The base of layer 2 is thicker south of the FZ than to the north; the rest of the crustal section is comparable in thickness (Figure 6). As on Figure 6, the shaded region again indicates the range of depths to the top of layer 3. Note the difference in the seafloor depth across the FZ. Thinning of the crust under the FZ is assumed following Shor et al.'s [1970] refraction results east of the Hawaiian Islands.

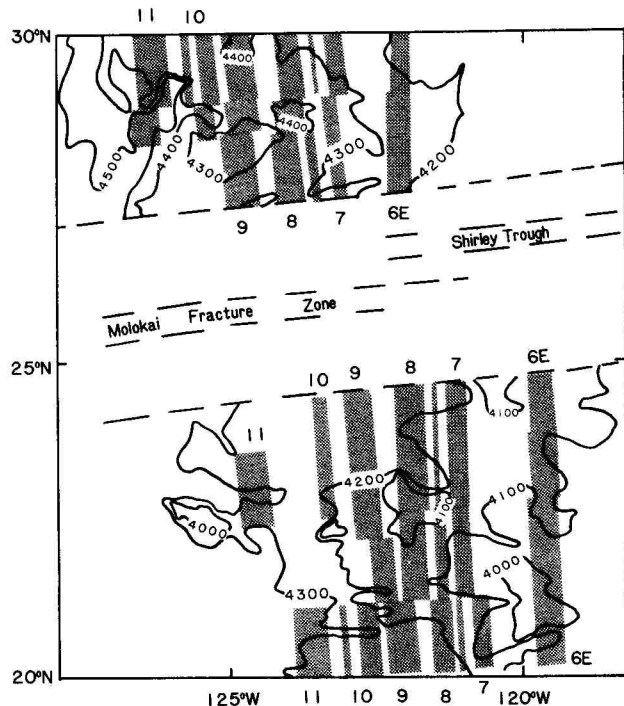


Fig. 12. Bathymetry (in meters) of the East Pacific Ocean across the Molokai FZ with magnetic anomalies 6-11 superimposed as numbered shaded rectangles (modified from Klitgord and Mammerickx [1982]). Note the differences in water depth across the Molokai FZ for seafloor having similar ages.

refraction studies conducted north of the Molokai FZ. Both the Fanfare experiment on 15 Ma crust near Guadelupe Island (118°30'W, 29°N) [Spudich and Orcutt, 1980] and the NEPAC seismic experiment on 60 Ma crust at longitude 148°W [Kempner and Gettrust, 1982], determined a crustal thickness in agreement with that determined for profiles obtained north of Oahu. This favorable comparison suggests, in agreement with the results of McClain [1981], that crustal thickening with age is not found in the Pacific ocean for seafloor older than 15 Ma.

To determine whether consistent differences in crustal thickness across the Molokai FZ are present elsewhere in the East Pacific, we converted the seismic velocities to densities using empirical relations given by Christensen and Salisbury [1975]. Assuming isostatic balance and depending on the assumed mantle density, 3.3-3.4 g/cm³, the calculated difference in seafloor depth for crust having the same age ranges between 150 and 208 m. (A similar calculation shows that the predicted differences in free air gravity and in the geoid heights across the Molokai FZ are negligible.) The predicted difference in seafloor depth is comparable in magnitude with the average observed difference in seafloor depth across the Molokai FZ for seafloor with similar ages (e.g., anomalies 6-11 (Figure 12) and 25-32). We cannot test the prediction of different seafloor depth across the Molokai FZ near the study area because the Hawaiian swell has obscured the seafloor age-to-depth relation near Oahu.

Klein and Langmuir [1987] report a correlation between the chemistry of mid-oceanic ridge

basalts, the axial depth of these ridges, and the crustal thickness in the vicinity of the ridge crest. This correlation, they explain, is due to variations in upper mantle temperatures below different segments of the mid-oceanic ridge (MOR). Differing volumes of partial melt are produced at different MOR segments when the geotherms, assumed to follow the mantle adiabat, intersect the mantle solidus at different depths. The adiabat having a higher initial temperature intersects the solidus deeper in the mantle, leading to a larger volume of melt.

Assuming that the observed differences in crustal structure north and south of Oahu were generated during crustal formation, one could explain these differences as reflecting thermally induced compositional variations between two segments of the mid-oceanic ridge. In particular, this model would predict that a lower-temperature mantle adiabat under the ridge segment supplies magma with lower temperatures and higher normative plagioclase contents, which produces a thinner crustal section [Klein and Langmuir, 1987]. Consequently, the crustal section may be affected in the following ways: magma within the crustal magma chamber would have a lower density (and seismic velocity) due to the enrichment in plagioclase components, and the crust will have fewer extrusives and late stage differentiates (thinner layer 2) due to the smaller volume of magma supply.

These characteristics are in accord with the seismic refraction features observed near Oahu, namely, both a slightly lower average velocity within layer 3 (suggested from forward modeling) and a thinner crust (due mainly to a thinner lower layer 2) are observed north of Oahu. The lower part of layer 2 represents late differentiates in the upper portions of the magma chamber and the crystallized liquid compositions which were extracted from this magma chamber, while layer 3 represents the magma chamber itself [Salisbury and Christensen, 1978]. Hence, we explain the crustal variations observed at the 60-80 Ma Pacific crust near Hawaii as being generated by variations in the thermal regime of the upper mantle under different segments of the ancestral mid-oceanic ridge. This hypothesis does not predict any detectable variations in the composition and seismic character of the upper mantle because the amount of melting in the upper mantle is too small (5-20 percent) [Klein and Langmuir, 1987].

The agreement between predicted and observed seafloor depth variations across the Molokai FZ east of the Hawaiian Islands has important implications for the physics of spreading centers. It suggests that thermal perturbations in the upper mantle underlying the ancestral Pacific ridge crest, of about 25° [Klein and Langmuir, 1987], were stable over a period of 50 m.y. It also suggests the existence of a significant difference, about 14 percent, in the total crustal volume generated at different spreading cell segments along the same ridge.

In addition to our study, other recent seismic studies provide evidence for midcrustal and lower crustal reflections from the oceanic crust in the western North Atlantic Ocean and the Pacific Ocean. Using wide-aperture two-ship profiling and large (54 L) airgun arrays, the NAT Study Group [1985] was able to map a subhorizontal diffractive lower crustal reflector in Mesozoic

age crust they termed "Horizon R." Upon post-stack migration "Horizon R" is seen more clearly as the top of deeper events dipping 20-40 degrees toward the spreading center and merging with the Moho reflection [McCarthy and Mutter, 1986], in analogy to a lower crustal event on synthetic reflection seismograms for a model of the Bay of Islands ophiolite [Collins et al., 1986; McCarthy and Mutter, 1986]. In the ophiolite models the lower crustal reflections are produced by interbedded cumulate gabbros and ultramafics. Alternatively, at least some of these reflections may originate from listric faults which formed near the ancestral spreading center. These faults may be reflective due to serpentinization of the surrounding lower crust by fluids migrating along the fault planes. Further support for this interpretation is provided by the observation that in places these reflections can be traced through the entire crust to offsets in the sediment-basement interface. The reflections observed near Oahu are similar to those observed in the North Atlantic in that they also have a predominant dip toward the ancestral spreading center but are different in that they cannot be clearly seen to shoal into and merge with the Moho reflection. Our ESP velocity-depth models (Table 2) suggest that the reflection at 7.5 s is located within the middle of layer 3.

On the basis of our ESP solutions and drilling results from Deep Sea Drilling Project hole 504B [Anderson et al., 1982], the discontinuous, undulating shallow event 0.6-1.0 s (1-2 km) into the igneous crust near Oahu may originate from the laterally variable extrusive lava/sheeted dyke contact. The observation of similar reflection events in the Cascadia basin in the northeast Pacific [Clowes and Knize, 1979], at the East Pacific Rise [Detrick et al., 1987], and now in the mid-Pacific (this study) suggests that the crustal accretion processes responsible for these reflectors are similar throughout the world's ocean basins having a wide variety of seafloor spreading rates.

Summary and Conclusions

A significant difference (1-2+1 km) in the thickness of the oceanic crust north and south of Oahu is observed on multichannel seismic refraction profiles. Tau-p stacks, tau-sum inversions, and forward modeling of several ESPs suggest that this crustal difference occurs primarily in layer 2 (Figures 3, 6, and 11). This difference is attributed to variations in crustal structure across the Molokai FZ. The total crustal thickness north of Oahu is compatible with other refraction experiments on younger crust north of the Molokai FZ, indicating no significant thickening of the oceanic crust with age past 15 Ma. Provided that the oceanic crust is isostatically compensated, the observed differences in crustal thickness should produce elevation differences of the seafloor across the Molokai FZ of about 150-200 m for seafloor of similar age. Elevation differences of this size are observed in the east Pacific along magnetic anomalies 6-11 and 25-32, suggesting that a significant difference in crustal thickness between the two segments of oceanic crust has been maintained from about 80 Ma to about 15 Ma. It seems most reasonable to explain these variations by processes operating along the ridge crest. The

decrease in total crustal and layer 2 thicknesses and the possible lowering of layer 3 velocities are all compatible with a magma supply having a lower temperature and a higher normative plagioclase contents north of the Molokai FZ than south of the FZ [Klein and Langmuir, 1987]. Hence the variations in crustal structure of the Pacific plate near Hawaii may be interpreted as evidence for spatial variations in the paleotemperatures in the upper mantle beneath the ancestral ridge crest which formed the Pacific plate.

Intracrustal reflections from approximately 1.6 s beneath the sediment-basement contact are best observed to the south of Oahu. On the basis of the ESP solutions, these reflections are located within layer 3 and lie well above the reflection Moho. The relative frequency content and stacking velocities of these reflections are compatible with those expected for lower crustal reflections, and the reflections are similar in character to those in Mesozoic age crust of the western North Atlantic Ocean [NAT Study Group, 1985]. Shallower isolated reflections inferred to originate from the transition between extrusive basalts and the sheeted dykes within layer 2 are also observed and, when combined with observations from other seismic studies [Grow and Markl, 1977; Clowes and Knize, 1979; McCarthy and Mutter, 1986; Detrick et al., 1987], suggest that this boundary may be more generally mappable using seismic reflection profiling than previously realized.

The results reported within this paper, as well as those reported from elsewhere [NAT Study Group, 1985; Detrick et al., 1987], demonstrate the unique capability of multichannel seismic reflection/refraction experiments to image complex crustal structure in detail. Our conclusions could be tested by performing a similar study along a N-S transect across the Molokai FZ to the east of Oahu where the magnetic anomalies are well developed and the locations of the small-offset FZ are well mapped.

Acknowledgments. We thank P. Buhl and J. Alsop and the rest of the Multichannel Seismic group at Lamont-Doherty Geological Observatory (LDGO) for their assistance in the processing of the ESP and CDP data and W. Kohler for writing software for the digitization of travel times. E. Geist plotted the CDP sections and performed filter tests and migration of CDP profile 330 shown here. W. Haxby and M. Weigel provided the Seasat-derived gravity map of Hawaii. We thank P. Buhl and E. Vera for many helpful discussions. We thank J. Collins, E. Goodwin, J. McCarthy, W. Mooney, J. Mutter, and A. B. Watts for careful reviews of earlier drafts of this manuscript. The final version of this paper benefited from critical reviews by G. Moore, an anonymous reviewer, and J. Orcutt. This work was supported by National Science Foundation grants OCE81-171210 (Hawaii Institute of Geophysics), OCE84-43349 (Woods Hole Oceanographic Institution), and OCE85-14073 (LDGO) and the U.S. Geological Survey, Branch of Seismology. Lamont-Doherty Geological Observatory contribution 4210.

References

- Anderson R. N., J. Honnorez, K. Becker, A. C. Adamson, J. C. Alt, R. Emmermann, P. D.

- Kempton, H. Kinoshita, C. Laverne, M. J. Mottl, and R. L. Newmark, DSDP hole 504B, the first reference section over 1 km through layer 2 of the oceanic crust, Nature, **300**, 589-594, 1982.
- Atwater, T., and H. W. Menard, Magnetic lineations in the northeast Pacific, Earth Planet. Sci. Lett., **7**, 445-450, 1970.
- Bratt, S. R., and G. M. Purdy, Structure and variability of oceanic crust on the flanks of the east Pacific Rise between 11° and 13°N, J. Geophys. Res., **89**, 6111-6125, 1984.
- Brocher, T. M., and U. S. ten Brink, Variations in oceanic layer 2 elastic velocities near Hawaii and their correlation to lithospheric flexure, J. Geophys. Res., **92**, 2647-2661, 1987.
- Cann, J. R., A model for oceanic crustal structure developed, Geophys. J. R. Astron. Soc., **39**, 169-187, 1974.
- Chapman, C. H., A new method for computing synthetic seismograms, Geophys. J. R. Astron. Soc., **54**, 481-518, 1978.
- Chase, T. E., M. W. Menard, and J. Mammerickx, Bathymetry N. Pac., charts 7 and 8, Scripps Inst. of Oceanogr., San Diego, Calif., 1970.
- Christensen, N. I., Ophiolites, seismic velocities and oceanic crustal structure, Tectonophysics, **47**, 131-137, 1978.
- Christensen, N. I., and M. H. Salisbury, Structure and constitution of the lower oceanic crust, Rev. Geophys., **13**, 57-86, 1975.
- Clowes, R. M., and S. Knize, Crustal structure from a marine seismic survey off the west coast of Canada, Can. J. Earth Sci., **16**, 1265-1280, 1979.
- Collins, J. A., T. M. Brocher, and J. F. Karson, Two-dimensional seismic reflection modeling of the oceanic crust/mantle transition in the Bay of Islands ophiolite complex, J. Geophys. Res., **91**, 12,520-12,538, 1986.
- Detrick, R. S., J. S. Madsen, P. Buhl, J. C. Mutter, E. Vera, J. Orcutt, and T. Brocher, Multichannel seismic imaging of an axial magma chamber along the East Pacific Rise 90N and 130, Nature, **326**, 35-42, 1987.
- Diebold, J. B., and P. L. Stoffa, The travel-time equation, tau-p mapping and inversion of common midpoint data, Geophysics, **46**, 238-254, 1981.
- Fornari, D. J., and J. F. Campbell, Submarine topography around the Hawaiian islands, Volcanism in Hawaii, vol. 1, edited by R. W. Decker, T. L. Wright, and P. H. Stauffer, U.S. Geol. Surv. Prof. Pap., **1350**, 109-124, 1987.
- Fox, J. P., and J. B. Stroup, The plutonic foundation of the oceanic crust, in The Sea, vol. 7, edited by C. Emiliani, pp. 119-218, John Wiley, New York, 1981.
- Furumoto, A. S., G. P. Woollard, J. F. Campbell, and D. M. Hussong, Variation in the thickness of the crust in the Hawaiian Archipelago, in The Crust and Upper Mantle of the Pacific Area, Geophys. Monogr. Ser., vol. 12, edited by L. Knopoff, C. Drake, and P. Hart, pp. 94-111, AGU, Washington, D. C., 1968.
- Grow, J. A., and R. G. Markl, IPOD-USGS multichannel seismic reflection profile from Cape Hatteras to the Mid-Atlantic Ridge, Geology, **5**, 625-630, 1977.
- Kempner, W. C., and J. F. Gettrust, Ophiolites, synthetic seismograms, and ocean crustal structure, 1, Comparison of ocean bottom seismometer data and synthetic seismograms for the Bay of Islands ophiolite, J. Geophys. Res., **87**, 8447-8462, 1982.
- Klein, E. M., and C. H. Langmuir, Global correlations of ocean ridge basalt chemistry with axial depth and crustal thickness, J. Geophys. Res., **92**, 8089-8115, 1987.
- Klitgord, K. M., and J. Mammerickx, Northern East Pacific Rise: Magnetic anomaly and bathymetric framework, J. Geophys. Res., **87**, 6725-6750, 1982.
- Malahoff, A., and G. G. Woollard, Magnetic and tectonic trends over the Hawaiian Ridge, in The Crust and Upper Mantle of the Pacific Area, Geophys. Monogr. Ser., vol. 12, edited by L. Knopoff, C. Drake, and P. Hart, pp. 241-276, AGU, Washington, D. C., 1968.
- McCarthy, J., and J. C. Mutter, Relict magma chamber structures preserved within the Mesozoic North Atlantic crust, Eos Trans. AGU, **67**, 1083, 1986.
- McClain, J., On long-term thickening of the oceanic crust, Geophys. Res. Lett., **8**, 1191-1194, 1981.
- NAT Study Group, North Atlantic Transect: A wide aperture, two-ship multichannel seismic investigation of the oceanic crust, J. Geophys. Res., **90**, 10,321-10,341, 1985.
- Purdy, G. M., and J. I. Ewing, Seismic structure of the ocean crust, in The Geology of North America: The Western Atlantic Region, DNAG Ser., vol. 1, edited by B. E. Tucholke and P. R. Vogt, pp. 313-331, Geological Society of America, Boulder, Colo., 1986.
- Salisbury, M. H., and N. I. Christensen, The seismic velocity structure of a traverse through the Bay of Islands ophiolite complex, Newfoundland, and exposure of oceanic crust and upper mantle, J. Geophys. Res., **83**, 805-817, 1978.
- Shor, G. G., H. W. Menard, and R. W. Raitt, II, Regional observations, I, Structure of the Pacific Basin, in The Sea, edited by A. E. Maxwell, vol. 4, pp. 3-27, John Wiley, New York, 1970.
- Spudich, P., and J. Orcutt, Petrology and porosity of an oceanic crustal site: Results from wave form modeling of seismic refraction data, J. Geophys. Res., **85**, 1409-1433, 1980.
- ten Brink, U. S., Lithospheric flexure and Hawaiian volcanism: A multichannel seismic perspective, Ph.D. thesis, Columbia Univ., New York, 1986.
- ten Brink, U. S. and T. M. Brocher, Multichannel seismic evidence for a subcrustal intrusive complex under Oahu and a model for Hawaiian volcanism, J. Geophys. Res., **92**, 13,687-13,707, 1987.
- Tsai, C. J., An analysis leading to the reduction of scattered noise on deep marine seismic records, Geophysics, **49**, 17-26, 1984.
- Watts, A. B., U. S. ten Brink, P. Buhl, and T. M. Brocher, A multichannel seismic study of lithospheric flexure across the Hawaiian-Emperor seamount chain, Nature, **315**, 105-111, 1985.
- T. M. Brocher, U.S. Geological Survey, MS 977, 345 Middlefield Road, Menlo Park, CA 94025.
U. S. ten Brink, Department of Geophysics, Stanford University, Stanford, CA 94305.

(Received January 5, 1987;
revised September 17, 1987;
accepted September 17, 1987.)